



Schweizerischer Erdbebedienst  
Service Sismologique Suisse  
Servizio Sismico Svizzero  
Swiss Seismological Service

**ETH** zürich

---

# **Riehen - Erlensträsschen (SRHE)**

## **SITE CHARACTERIZATION REPORT**

**Clotaire MICHEL, Carlo CAUZZI, Manuel HOBIGER**

**Valerio POGGI, Jan BURJANEK, Donat FÄH**

---



Sonneggstrasse 5 CH-8092 Zürich Switzerland; E-mail: [clotaire.michel@sed.ethz.ch](mailto:clotaire.michel@sed.ethz.ch)

Last modified : January 5, 2015

## Abstract

Ambient vibration array measurements were performed to characterize the site Riehen Erlensträsschen, in centre of Riehen town. The site, where the new station SRHE of the Swiss Strong Motion Network was installed, is located on an alluvial terrace of the Wiese North to Basel. The new station was installed in the frame of the Basel Erdbebenvorsorge project. In order to characterize the velocity profile under the station, array measurements with a 170 m aperture were performed. The measurements were successful and allowed deriving a velocity model for this site that is compared to geological borehole data. We found a first layer of approximately 20 m with velocities of about 400 m/s corresponding to the alluvial terrace. Below, the velocity in the molasse alsacienne is linearly increasing down to 100 m depth where it reaches 1000 m/s. The velocity is then not varying much down to the bedrock at about 500 m depth. This interface with the Mesozoic rock is producing the fundamental peak in the ellipticity at 0.6 Hz.

$V_{s,30}$  is 373 m/s, which would corresponds to ground type B in the Eurocode 8, at the limit with type C [CEN, 2004] and E for the SIA261, although C would also be realistic [SIA, 2003]. The theoretical 1D SH transfer function and impedance contrast of the quarter-wavelength velocity computed from the inverted profiles show significant amplifications at clearly defined resonance frequencies. Recordings on the new station will allow to compare to these simple models.

## Contents

|          |  |           |
|----------|--|-----------|
| <b>1</b> | <b>Introduction</b>  | <b>4</b>  |
| <b>2</b> | <b>Geology</b>   | <b>5</b>  |
| <b>3</b> | <b>Experiment description</b>                                  | <b>6</b>  |
| 3.1      | Ambient Vibrations . . . . .                                   | 6         |
| 3.2      | Equipment . . . . .  | 6         |
| 3.3      | Geometry of the arrays . . . . .                               | 6         |
| 3.4      | Positioning of the stations . . . . .                          | 7         |
| <b>4</b> | <b>Data quality</b>  | <b>8</b>  |
| 4.1      | Usable data . . . . .  | 8         |
| 4.2      | Data processing . . . . .                                      | 8         |
| <b>5</b> | <b>H/V processing</b>  | <b>9</b>  |
| 5.1      | Processing method and parameters . . . . .                     | 9         |
| 5.2      | Results . . . . .  | 9         |
| 5.3      | Polarization analysis . . . . .                                | 11        |
| <b>6</b> | <b>Array processing</b>  | <b>13</b> |
| 6.1      | Processing methods and parameters . . . . .                    | 13        |
| 6.2      | Obtained dispersion curves . . . . .                           | 13        |
| <b>7</b> | <b>Inversion and interpretation</b>                            | <b>15</b> |
| 7.1      | Inversion . . . . .  | 15        |
| 7.2      | Travel time average velocities and ground type . . . . .       | 19        |
| 7.3      | SH transfer function and quarter-wavelength velocity . . . . . | 19        |
| <b>8</b> | <b>Conclusions</b>   | <b>23</b> |
|          | <b>References</b>  | <b>25</b> |

# 1 Introduction

The station SRHE (Riehen - Erlensträsschen) is part of the dense array of the Swiss Strong Motion Network (SSMNet) in Basel. SRHE has been installed in the framework of the Basel Erdbebenvorsorge project in 2013 as a new station. This project includes also the site characterization. Passive array measurements have been selected as a standard tool to investigate these sites. An array measurement campaign was carried out on 7th March 2014 in the area of the primary school, in the centre of the town of Riehen (Fig. 1), with a centre close to SRHE, in order to characterize the velocity profile under this station. This station is located on an alluvial terrace of the Wiese river. This report presents the measurement setup, the results of the H/V analysis and of the array processing of the surface waves (dispersion curves). Then, an inversion of these results into velocity profiles is performed. Standard parameters are derived to evaluate the amplification at this site.

| Canton      | City   | Location        | Station code | Site type        | Slope        |
|-------------|--------|-----------------|--------------|------------------|--------------|
| Basel Stadt | Riehen | Erlensträsschen | SRHE         | Alluvial terrace | Slight slope |

Table 1: Main characteristics of the study-site.

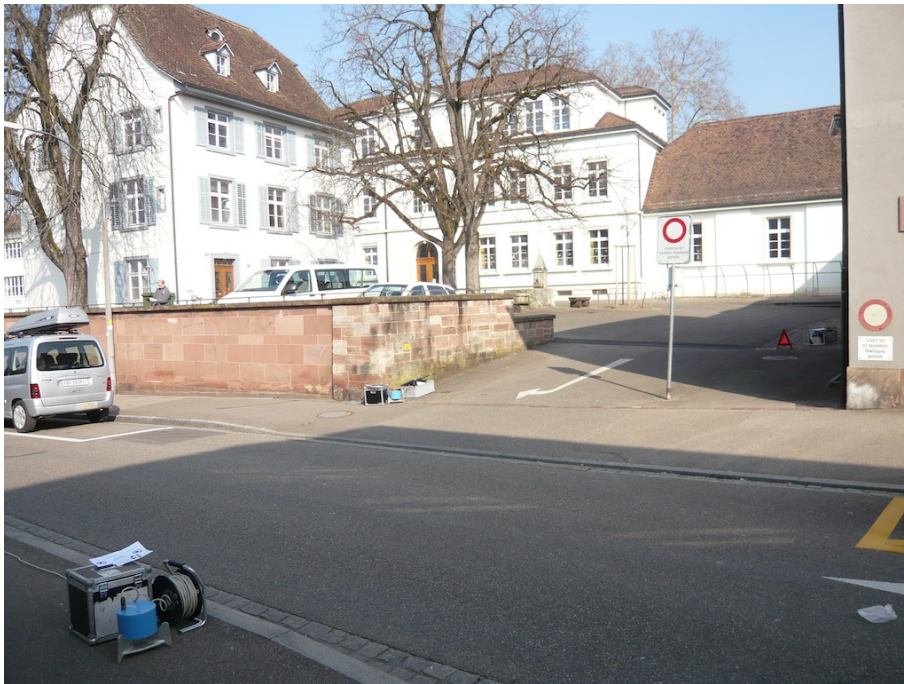


Figure 1: Picture of the site.

## 2 Geology

The geological map indicates (Fig. 2) that the site located on an alluvial terrace of the Wiese river. The borehole Riehen 1 [Hauber, 1991], located 170 m North is showing that the quaternary sediments are approximately 20 m thick and lay on the Molasse alsacienne layer (marls of Chattian age, Tertiary) down to 186 m depth. Below, the Meletta layers (silts of Rupelian age, Tertiary) are found down to 484 m depth. Below, the less thick layers of the Fischschiefer (schists), the Foraminifermergel (marls) and 50 m of Sannoisian marl lead to the base of the Tertiary at 556 m depth, laying on the Callovian rock (limestone). The station is located within the deepest part of the Rhine graben where resonance from Tertiary and Quaternary sediments is expected. Moreover, it is located in the St Jakob-Tüllingen syncline where deeper Tertiary sediments deposited, compared to the city-centre of Basel. According to the microzonation of Basel [Fäh and Huggenberger, 2006], the station is located in the zone Rheingraben-Ost, on Pleistocene sediments. In this zone, the microzonation is predicting amplifications of a factor of 2 to 3 in response spectrum.

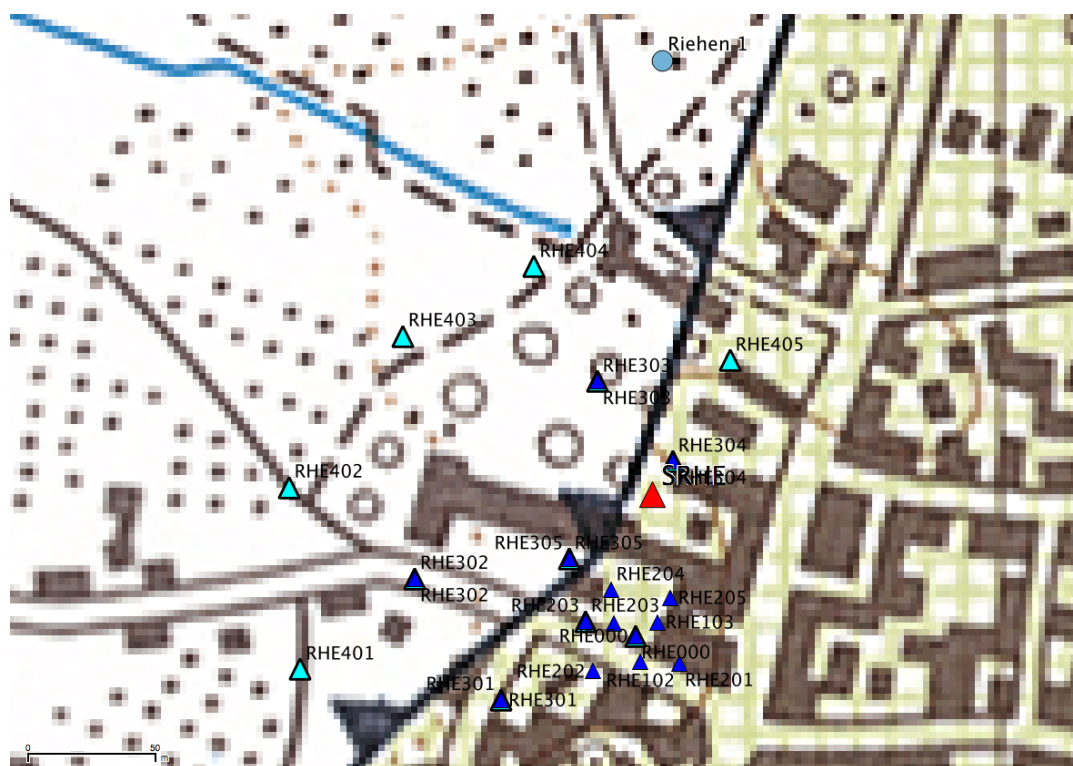


Figure 2: Geological map of the area of station SRHE including the array stations and the deep borehole Riehen 1. The white color refers to alluvia and the green crosshatched area to a lower alluvial terrace.

### 3 Experiment description

#### 3.1 Ambient Vibrations

The ground surface is permanently subjected to ambient vibrations due to:

- natural sources (ocean and large-scale atmospheric phenomena) below 1 Hz,
- local meteorological conditions (wind and rain) at frequencies around 1 Hz ,
- human activities (industrial machines, traffic...) at frequencies above 1 Hz [Bonney-Claudet et al., 2006].

The objective of the measurements is to record these ambient vibrations and to use their propagation properties to infer the underground structure. First, the polarization of the recorded waves (H/V ratio) is used to derive the resonance frequencies of the soil column. Second, the arrival time delays at many different stations are used to derive the velocity of surface waves at different frequencies (dispersion). The information (H/V, dispersion curves) is then used to derive the properties of the soil column using an inversion process.

#### 3.2 Equipment

For these measurements 11 Quanterra Q330 dataloggers named NR02 to NR12 and 14 Lennartz 3C 5 s seismometers were available (see Tab. 2). Each datalogger can record on 2 ports A (channels EH1, EH2, EH3 for Z, N, E directions) and B (channels EH4, EH5, EH6 for Z, N, E directions). Time synchronization was ensured by GPS. The sensors were placed on a metal tripod, in a 20 cm deep hole, when necessary, for better coupling with the ground.

| <b>Digitizer</b>   | <b>Model</b>   | <b>Number</b> | <b>Resolution</b>        |
|--------------------|----------------|---------------|--------------------------|
|                    | Quanterra Q330 | 11            | 24 bits                  |
| <b>Sensor type</b> | <b>Model</b>   | <b>Number</b> | <b>Cut-off frequency</b> |
| Velocimeter        | Lennartz 3C    | 14            | 0.2 Hz                   |

Table 2: Equipment used.

#### 3.3 Geometry of the arrays

Two array configurations were used. In the first configuration, 2 rings of 10 and 20 m radius around a central station as well as an array of five stations creating another ring of 60 m radius around station RHE305 for a total of 14 sensors; the second configuration includes the outer ring (plus the central station and 1 sensor of the first ring) and a semi-circular ring of 85 m radius with 12 sensors. The minimum inter-station distance and the aperture are therefore 10 and 120 m and 20 and 170 m, respectively. The experimental setup is displayed in Fig. 3. The final usable datasets are detailed in section 4.2.

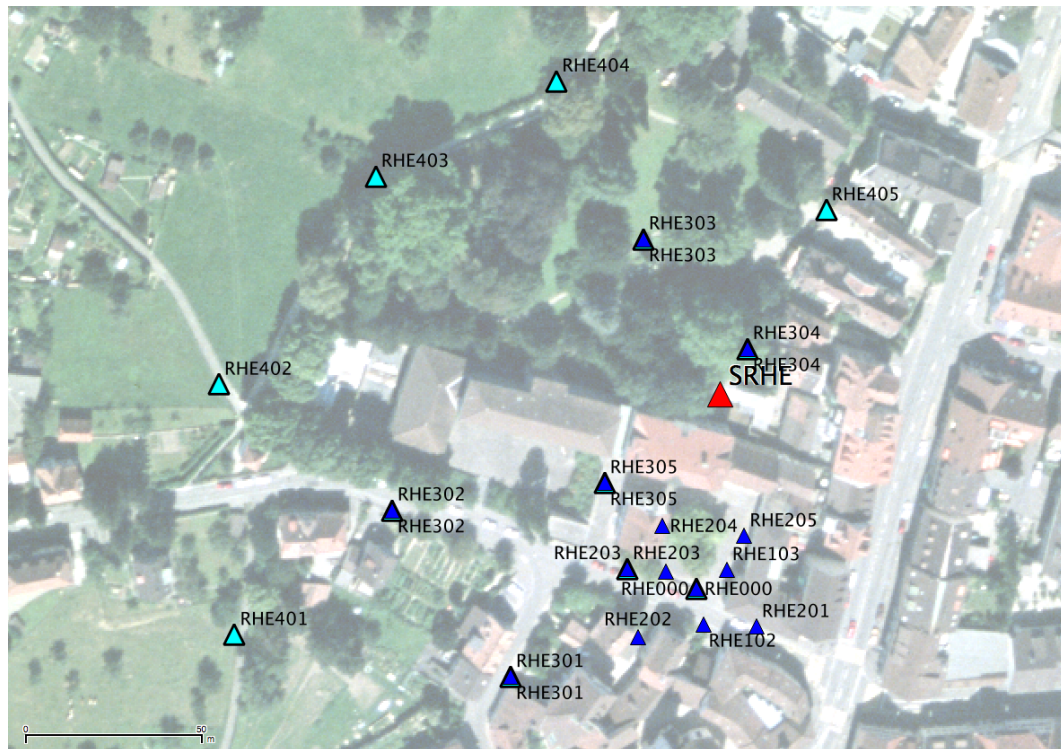


Figure 3: Geometry of the arrays. Deep blue triangles refer to the first configuration and triangles with thick edges refer to the second configuration.

### 3.4 Positioning of the stations

The sensor coordinates were measured using a differential GPS device (Leica Viva GS10), including only a rover station and using the Real Time Kinematic technique provided by Swisstopo. It allows an absolute positioning with an accuracy better than 6 cm on the Swissgrid. However, this accuracy was not reached at several points due to trees and buildings. The less accurate points were: RHE202 with 102 cm, RHE204 with 30 cm, RHE301 with 21 cm and RHE304 with 18 cm.

## 4 Data quality

### 4.1 Usable data

The largest time windows were extracted, for which all the sensors of the array were correctly placed and the GPS synchronization was ensured. N component of sensors RHE103 and RHE402 did not work due to a broken pin during the previous experiment. Recordings are generally consistent. Higher noise at high frequency is noticed for RHE304 due to a strange source that may be an animal (bird). RHE102 shows a slightly different behavior at low frequency. For the second configuration, higher noise levels are present at the array centre and in RHE405 (closer to the road). A large undamped peak can be noticed at 16.27 Hz with a source close to the array centre.

Orientations of the sensors were checked by maximizing the correlation with the central station at low frequencies [Poggi et al., 2012b]. Deviations lower than  $7^\circ$  were found for all points but RHE202 ( $14^\circ$ ). Original and rotated datasets are available for the 3C array analysis.

The characteristics of the datasets are detailed in Tab. 3.

### 4.2 Data processing

The data were first converted to SAC format including in the header the coordinates of the point (CH1903 system), the recording component and a name related to the position. The name is made of 3 letters characterizing the location (RHE here), 1 digit for the ring and 2 more digits for the number in the ring. Recordings were not corrected for the instrumental response.

| Dataset | Starting Date | Time  | Length  | $F_s$  | Min. inter-distance | Aperture | # of points |
|---------|---------------|-------|---------|--------|---------------------|----------|-------------|
| 1       | 2014/03/07    | 09:54 | 126 min | 200 Hz | 10 m                | 120 m    | 13          |
| 2       | 2014/03/07    | 12:36 | 122 min | 200 Hz | 20 m                | 170 m    | 11          |

Table 3: Usable datasets.

## 5 H/V processing

### 5.1 Processing method and parameters

In order to process the H/V spectral ratios, several codes and methods were used. The classical H/V method was applied using the Geopsy <http://www.geopsy.org> software. In this method, the ratio of the smoothed Fourier Transform of selected time windows are averaged. Tukey windows (cosine taper of 5% width) of 50 s long overlapping by 50% were selected. Konno and Ohmachi [1998] smoothing procedure was used with a b value of 60. The classical method computed using the method of Fäh et al. [2001] was also performed.

Moreover, the time-frequency analysis method [Fäh et al., 2009] was used to estimate the ellipticity function more accurately using the Matlab code of V. Poggi. In this method, the time-frequency analysis using the Wavelet transform is computed for each component. For each frequency, the maxima over time (10 per minute with at least 0.1 s between each) in the TFA are determined. The Horizontal to Vertical ratio of amplitudes for each maximum is then computed and statistical properties for each frequency are derived. A Cosine wavelet with parameter 9 is used. The mean of the distribution for each frequency is stored. For the sake of comparison, the time-frequency analysis of Fäh et al. [2001], based on the spectrogram, was also used.

The ellipticity extraction using the Capon analysis [Poggi and Fäh, 2010] (see section on array analysis) was also performed.

| Method              | Freq. band  | Win. length   | Anti-trig. | Overlap | Smoothing |
|---------------------|-------------|---------------|------------|---------|-----------|
| Standard H/V Geopsy | 0.2 – 20 Hz | 50 s          | No         | 50%     | K&O 60    |
| Standard H/V D. Fäh | 0.2 – 20 Hz | 30 s          | No         | 75%     | -         |
| H/V TFA D. Fäh      | 0.2 – 20 Hz | Specgram      | No         | -       | -         |
| H/V TFA V. Poggi    | 0.2 – 20 Hz | Cosine wpar=9 | No         | -       | No        |

Table 4: Methods and parameters used for the H/V processing.

### 5.2 Results

All points show exactly the same shape in their H/V below 5 Hz with a complex right flank (Fig. 4). The fundamental peak is broad with a first value of 0.44 Hz, but the average peak frequency value would rather be 0.6 Hz. This corresponds to the resonance of the deep Rhine graben.

Moreover, all the methods to compute H/V ratios are compared at the array centre on Fig. 5, in which the classical methods were divided by  $\sqrt{2}$  to correct from the Love wave contribution [Fäh et al., 2001]. The classical and TFA methods match well at high frequencies but large variations are observed at low frequencies. The 3C FK analysis (Capon method) does not have resolution down to the peak but matches perfectly at high frequency.

The fundamental peak at the SRHE station is therefore at 0.6 Hz, with a peak amplitude around 3 for the TFA methods.

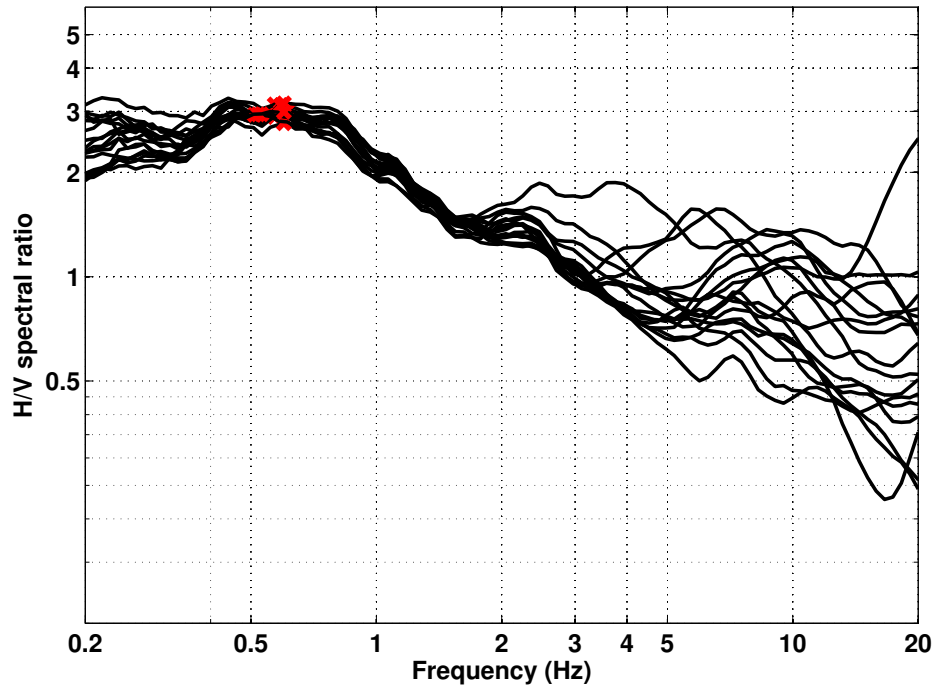


Figure 4: H/V spectral ratios (time-frequency analysis code V. Poggi).

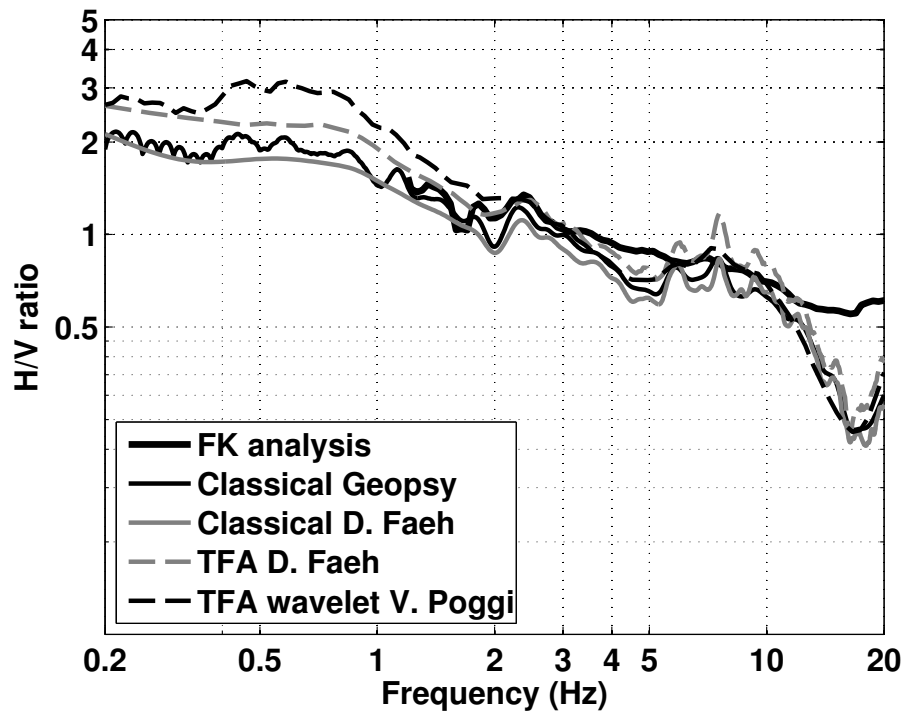


Figure 5: H/V spectral ratios for point RHE000 using the different codes. Classical methods were divided by  $\sqrt{2}$ .

Fig. 6 is showing the H/V ratios of points along a transverse cross section of the alluvial terrace. Points on the terrace show small amplitude secondary peaks above 5 Hz, whereas points on the alluvia, although located at a lower altitude, show a secondary peak at about 3 Hz with higher amplitude. The altitude difference is therefore not playing a significant role here. On the alluvia, the velocity contrast between the quaternary and the tertiary sediments is larger due to lower velocity sediments, inducing a larger peak at lower frequency. No information about the variation in the depth of these sediments can be retrieved, though.

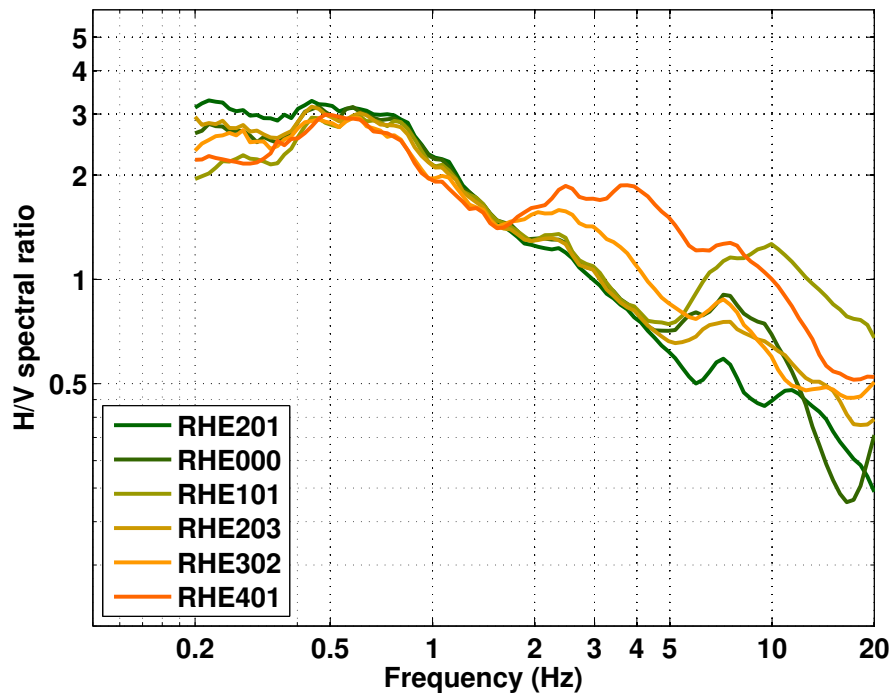


Figure 6: H/V spectral ratios for a cross-section of points traverse to the alluvial terrace. Points in green are on the terrace, orange on the slope and red on the alluvia.

### 5.3 Polarization analysis

Considering the shape of the Rhine basin, a 2D resonance could occur. Therefore, polarization analysis on the array data was performed using the method of Burjánek et al. [2010]. No points (Fig. 7) show a particular polarization at the resonance frequency. 2D resonance should therefore not occur at this location.

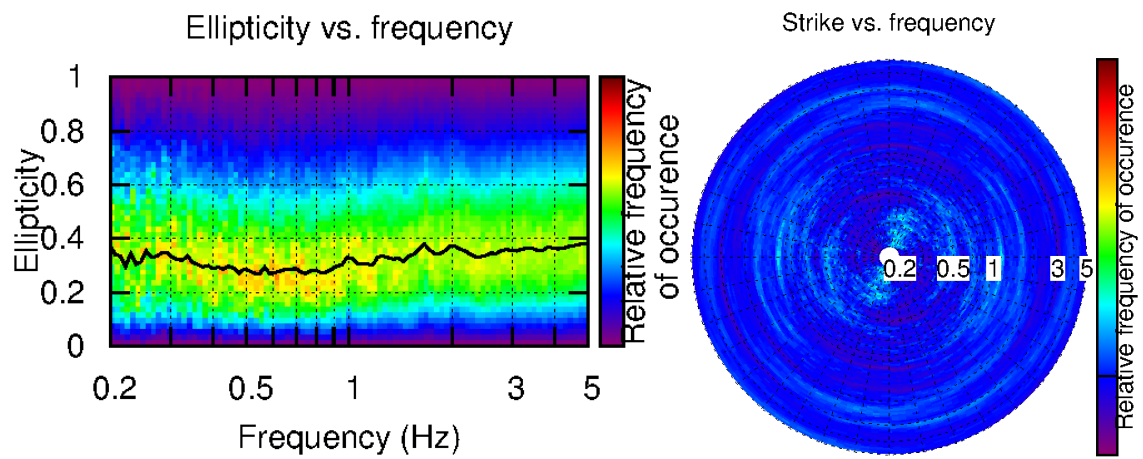


Figure 7: Polarization analysis at point RHE000. Left: Ellipticity (A trough in the ellipticity corresponds to polarized motion). Right: Strike of the polarization.

## 6 Array processing

### 6.1 Processing methods and parameters

The vertical components of the arrays were processed using the FK and the High-resolution FK analysis [Capon, 1969] using the Geopsy <http://www.geopsy.org> software. Better results were obtained using large time windows (300T). The results of computations of both datasets were merged to estimate the dispersion curves.

Moreover, a 3C array analysis [Fäh et al., 2008] was also performed using the `array_tool_3C` software [Poggi and Fäh, 2010]. It allows to derive Rayleigh and Love modes including the Rayleigh ellipticity. The results of computations of both datasets were merged to estimate the dispersion curves.

| Method  | Set | Freq. band | Win. length         | Anti-trig. | Overlap | Grid step  | Grid size   | # max. |
|---------|-----|------------|---------------------|------------|---------|------------|-------------|--------|
| HRFK 1C | 1   | 1 – 25 Hz  | 300T                | No         | 50%     | 0.001      | 0.6         | 5      |
| HRFK 1C | 2   | 1 – 25 Hz  | 300T                | No         | 50%     | 0.001      | 0.6         | 5      |
| HRFK 3C | 1   | 1 – 27 Hz  | Wav. 10<br>Tap. 0.2 | No         | 50%     | 200<br>m/s | 2000<br>m/s | 5      |
| HRFK 3C | 2   | 1 – 27 Hz  | Wav. 10<br>Tap. 0.2 | No         | 50%     | 200<br>m/s | 2000<br>m/s | 5      |

Table 5: Methods and parameters used for the array processing.

### 6.2 Obtained dispersion curves

In the 1C FK analysis, the fundamental Rayleigh mode could be picked between 1.6 Hz and 22 Hz (Fig. 8), including its standard deviation. The velocities are ranging from 1227 m/s at 1.6 Hz on the fundamental mode down to 285 m/s at 22 Hz.

Using the 3C analysis, the fundamental Rayleigh mode can be picked as well (Fig. 8). On the radial component the same mode is seen. On the transverse component, fundamental Love mode is picked in a similar frequency range as Rayleigh. The curve above 13 Hz is however less certain.

All picked curves are presented together on Fig. 9. The fundamental Rayleigh mode are identical for 1C and 3C analysis.

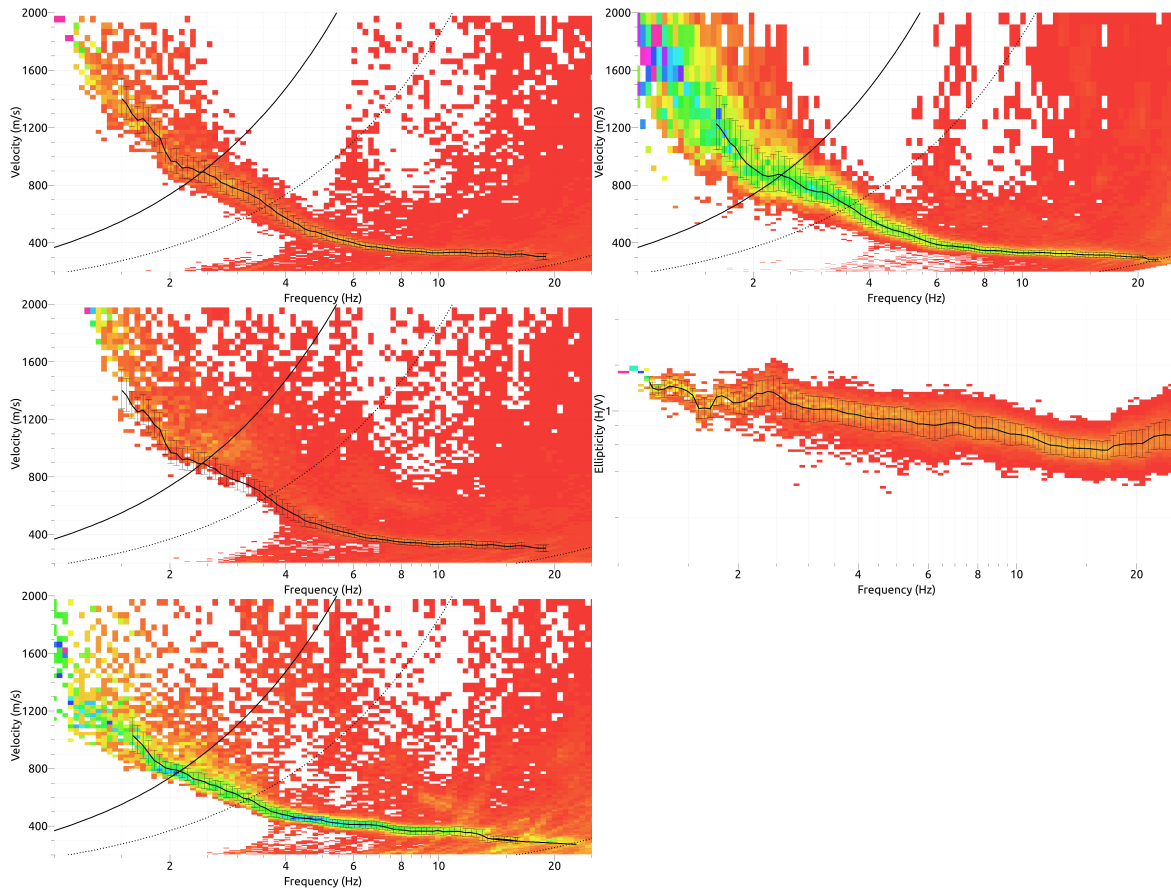


Figure 8: Dispersion curves and ellipticity obtained from the 3C and 1C array analyses (from top to bottom: vertical, radial, transverse components; left: 3C analysis; top right: 1C analysis; centre right: ellipticity).

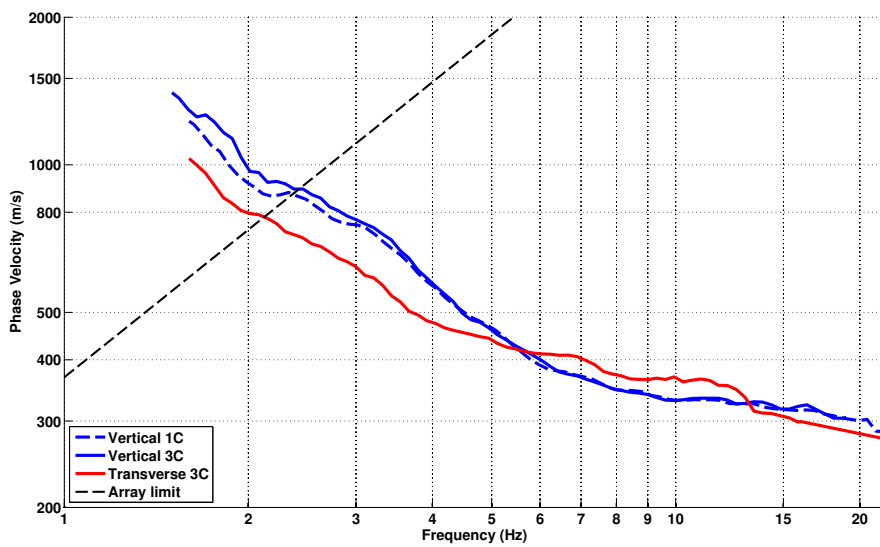


Figure 9: Picked dispersion curves from 1C and 3C FK methods.

## 7 Inversion and interpretation

### 7.1 Inversion

For the inversion, Rayleigh and Love fundamental mode dispersion curves between 2 and 21 Hz, as well as the ellipticity curve and the fundamental frequency at 0.6 Hz were used as simultaneous targets without standard deviation to avoid different weighting. The right flank of the second peak for the central point of the array was used as well to constrain better the upper part of the profiles. The Rayleigh curve from the 1C analysis was chosen. A weight of 0.3 was assigned to the ellipticity curve and 0.2 for the ellipticity peak. All curves were resampled using 50 points between 0.4 and 23 Hz in log scale.

The inversion was performed using the Improved Neighborhood Algorithm (NA) Wathelet [2008] implemented in the Dinver software. In this algorithm, the tuning parameters are the following:  $N_{s_0}$  is the number of starting models, randomly distributed in the parameter space,  $N_r$  is the the number of best cells considered around these  $N_{s_0}$  models,  $N_s$  is the number of new cells generated in the neighborhood of the  $N_r$  cells ( $N_s/N_r$  per cell) and  $It_{max}$  is the number of iteration of this process. The process ends with  $N_{s_0} + N_r * \frac{N_s}{N_r} * It_{max}$  models. The used parameters are detailed in Tab. 6.

| $It_{max}$ | $N_{s_0}$ | $N_s$ | $N_r$ |
|------------|-----------|-------|-------|
| 500        | 10000     | 100   | 100   |

Table 6: Tuning parameters of Neighborhood Algorithm.

The velocity was assumed to increase with depth. The Poisson ratio was inverted in each layer in the range 0.2-0.4. Allowing for larger values has been tested but leads to the same results. The density was assumed between 2000 and 2500 kg/m<sup>3</sup>. Inversions with free layer depths as well as fixed layer depths were performed. 4 layers are enough to explain most of the targets (dispersion and ellipticity), but more layers are used to smooth the obtained results and better explore the parameter space. 5 independent runs of 5 different parametrization schemes (4 and 6 layers over a half space and 11, 12 and 12 layers with fixed depth) were performed. For further elaborations, the best models of these 25 runs were selected (Fig. 13).

The first 5 m may have rather low velocity of 200 to 300 m/s but are not well constrained (Fig. 10 and Fig. 13). As expected, the first 20 to 30 m are unconsolidated sediments with velocities of about 400 m/s. They corresponds to the quaternary sediments from the alluvial terrace. Between 20 and 100 m, the velocity in the molasse is linearly increasing up to about 1000 m/s. Below, the velocity is only slightly increasing up to 1300 m/s down to the bedrock. A velocity inversion at the interface with the Meletta layers at 186 m cannot be constrained by our data. The bedrock depth is found between 450 and 550 m depth, which is coherent with the base of the Tertiary in the borehole at 556 m. The velocity in the bedrock is not constrained and assumed smaller than 2500 m/s.

When comparing to the target curves (Fig. 11 and Fig. 12), the dispersion curves are well represented. The peaks of the ellipticity curves are well reproduced as well, but the amplitude in-between the peaks is not matching.

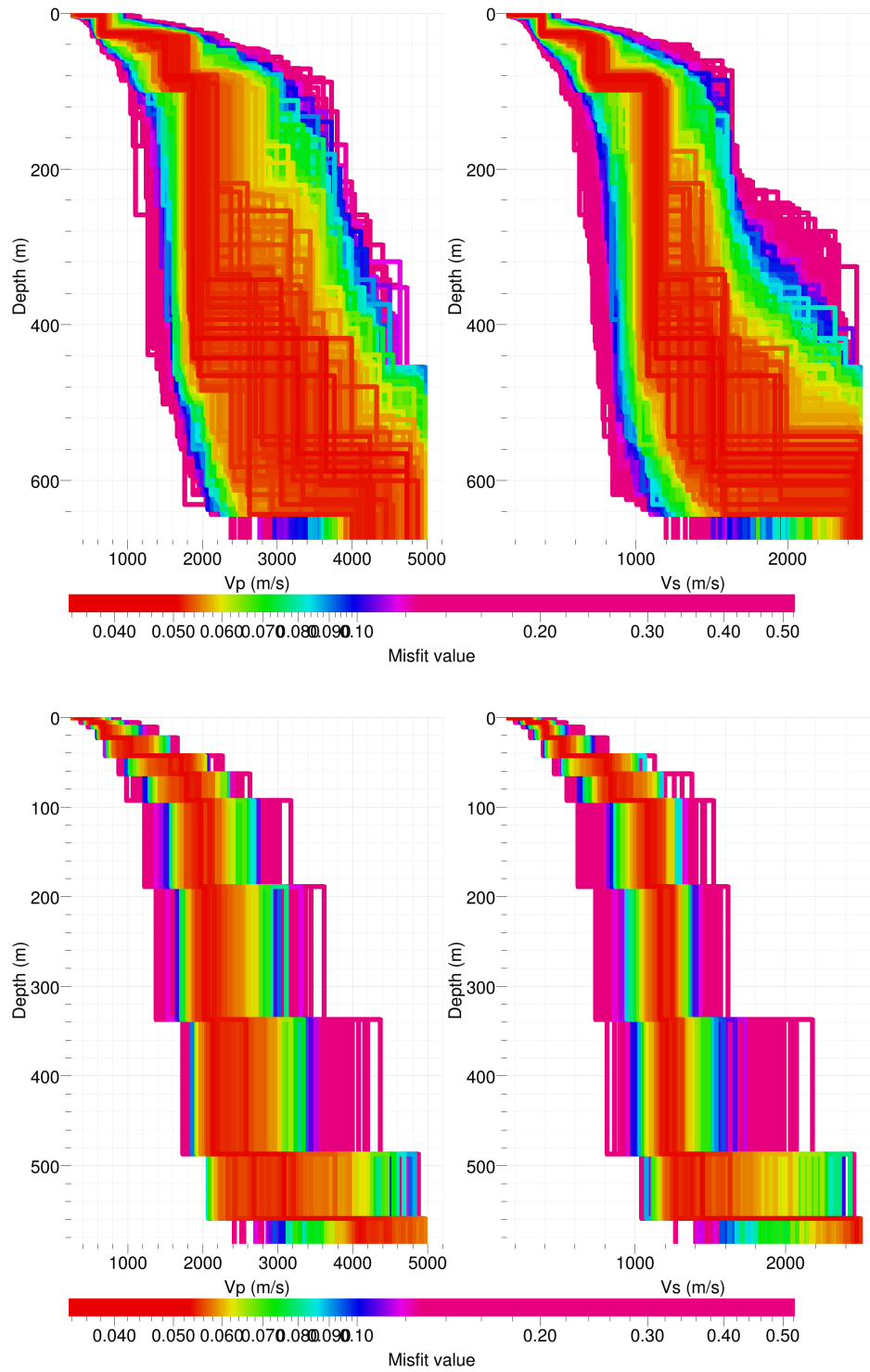


Figure 10: Inverted ground profiles in terms of  $V_p$  and  $V_s$ ; top: free layer depth strategy; bottom: fixed layer depth strategy.

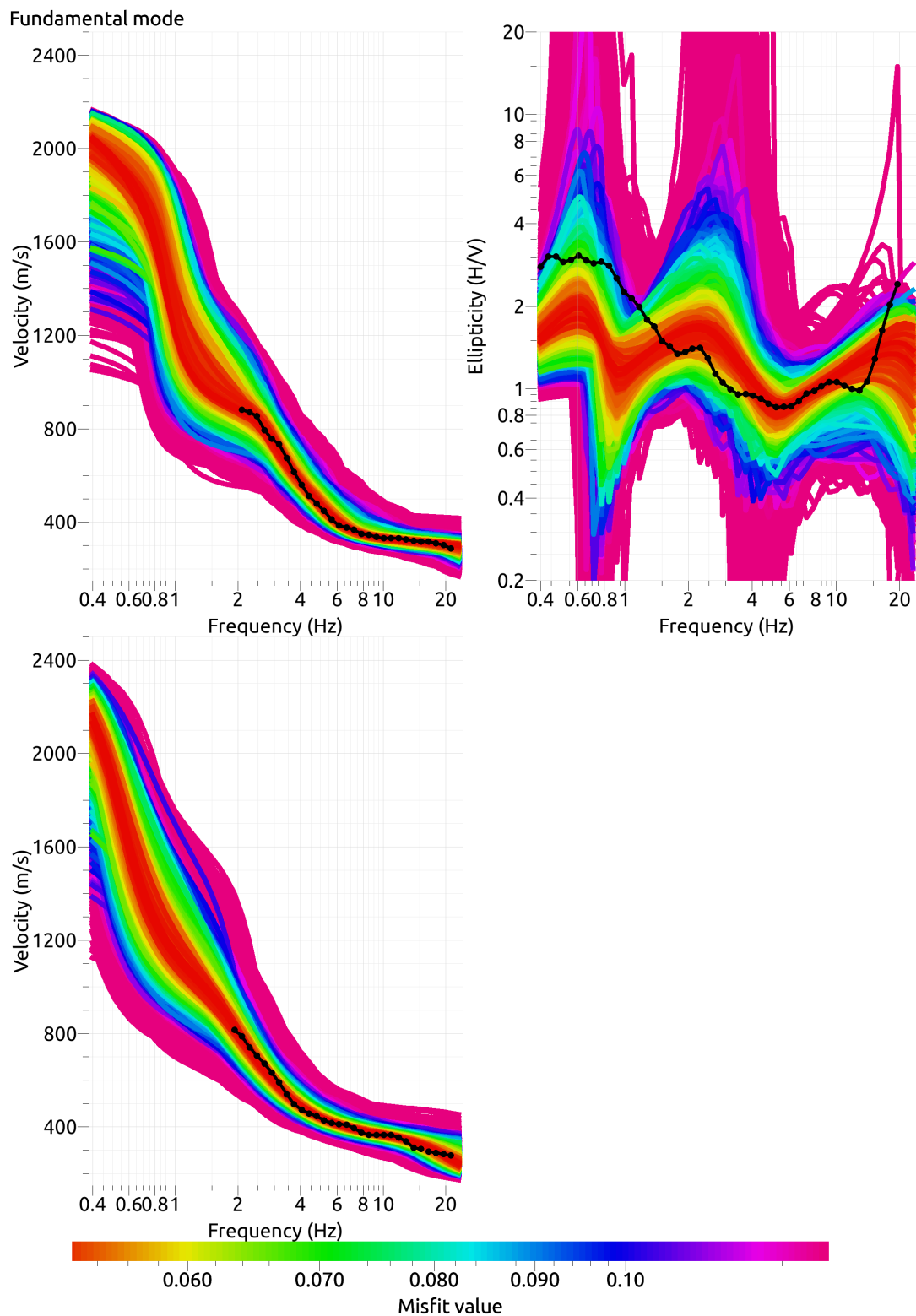


Figure 11: Comparison between inverted models and measured Rayleigh and Love modes and corresponding ellipticity, free layer depth strategy.

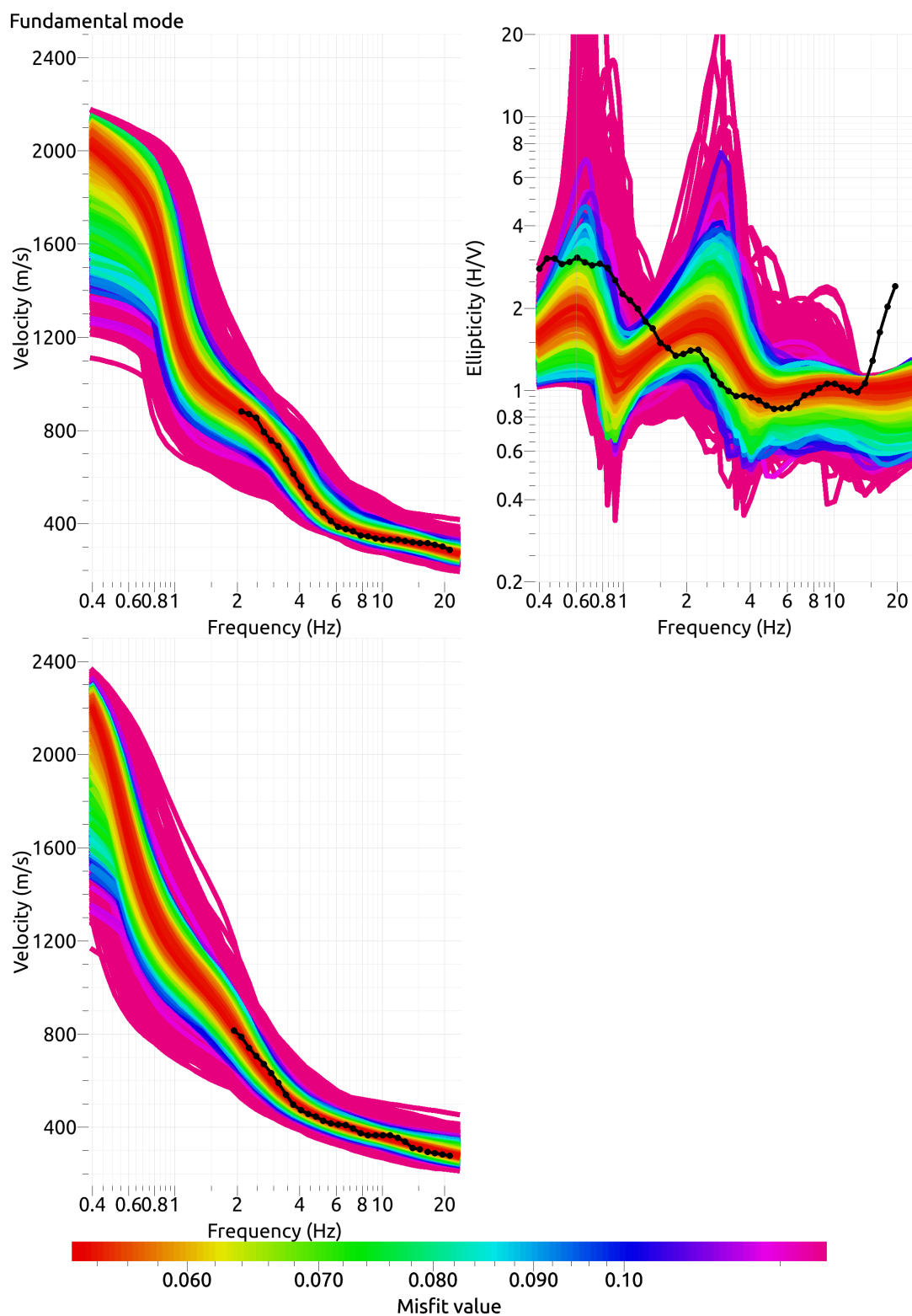


Figure 12: Comparison between inverted models and measured Rayleigh and Love modes and corresponding ellipticity, fixed layer depth strategy.

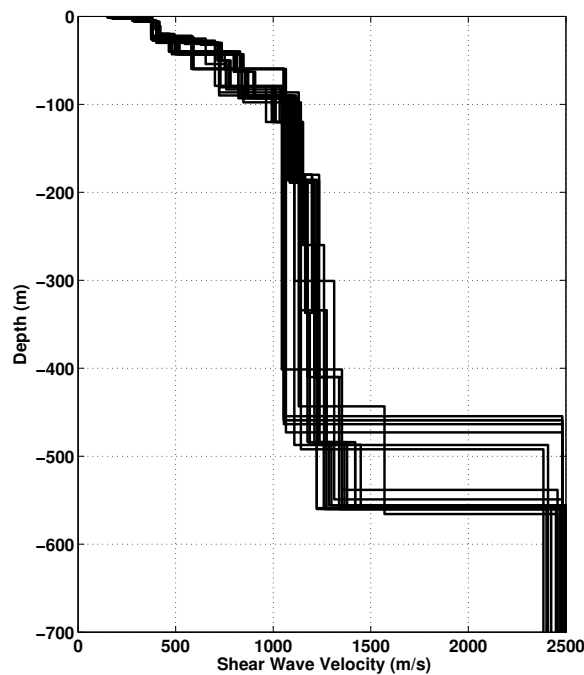


Figure 13:  $V_s$  ground profiles for the selected 25 best models.

## 7.2 Travel time average velocities and ground type

The distribution of the travel time average velocities at different depths was computed from the selected models. The uncertainty, computed as the standard deviation of the distribution of travel time average velocities for the considered models, is also provided, but it is not guaranteed that the full range of uncertainties is covered.  $V_{s,30}$  is found to be 373 m/s, which corresponds to class B in the Eurocode 8, close to class C [CEN, 2004]. For SIA261 [SIA, 2003], the first 20 m at 400 m/s on more consolidated sediments may classify this site in type E, though type C would be more reasonable considering the low velocity contrast.

## 7.3 SH transfer function and quarter-wavelength velocity

The quarter-wavelength velocity approach [Joyner et al., 1981] provides, for a given frequency, the average velocity at a depth corresponding to 1/4 of the wavelength of interest. It is useful to identify the frequency limits of the experimental data (minimum frequency in dispersion curves at 2 Hz and ellipticity peak at 0.6 Hz here). The results using this proxy show that the dispersion curves constrain the profiles down to 60 m and the ellipticity down to 370 m (Fig. 14). Moreover, the quarter wavelength impedance-contrast introduced by Poggi et al. [2012a] is also displayed in the figure. It corresponds to the ratio between two quarter-wavelength average velocities, respectively from the top and the bottom part of the velocity profile, at a given frequency [Poggi et al., 2012a]. It shows a trough (inverse shows a peak) at the resonance frequency.

|             | <b>Mean<br/>(m/s)</b> | <b>Uncertainty<br/>(m/s)</b> |
|-------------|-----------------------|------------------------------|
| $V_{s,5}$   | 249                   | 5                            |
| $V_{s,10}$  | 301                   | 3                            |
| $V_{s,20}$  | 342                   | 6                            |
| $V_{s,30}$  | 373                   | 9                            |
| $V_{s,40}$  | 410                   | 7                            |
| $V_{s,50}$  | 446                   | 6                            |
| $V_{s,100}$ | 588                   | 7                            |
| $V_{s,150}$ | 694                   | 6                            |
| $V_{s,200}$ | 766                   | 7                            |

Table 7: Travel time averages at different depths from the inverted models. Uncertainty is given as one standard deviation from the selected profiles.

Moreover, the theoretical SH-wave transfer function for vertical propagation [Roesset, 1970] is computed from the inverted profiles. It is compared to the quarter-wavelength amplification [Joyner et al., 1981] that however cannot take resonances into account (Fig. 15). In this case, the models are predicting a peaky amplification up to a factor of 5 at several resonance peaks between 1 and 4 Hz.

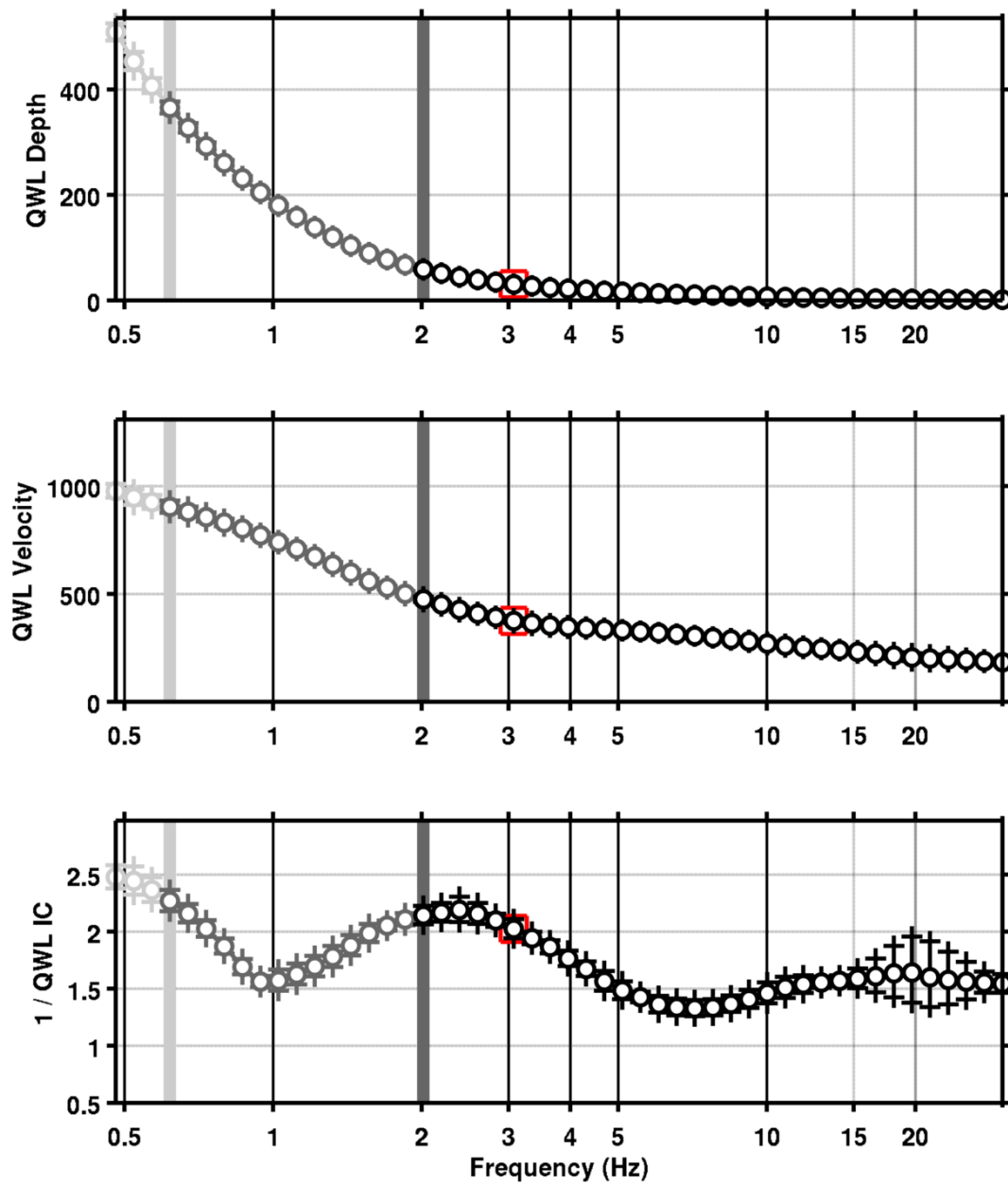


Figure 14: Quarter wavelength velocity representation of the velocity profile (top: depth, centre: velocity, bottom: inverse of the impedance contrast). Black curve is constrained by the dispersion curves, light grey is not constrained by the data. Red square is corresponding to  $V_{s,30}$ .

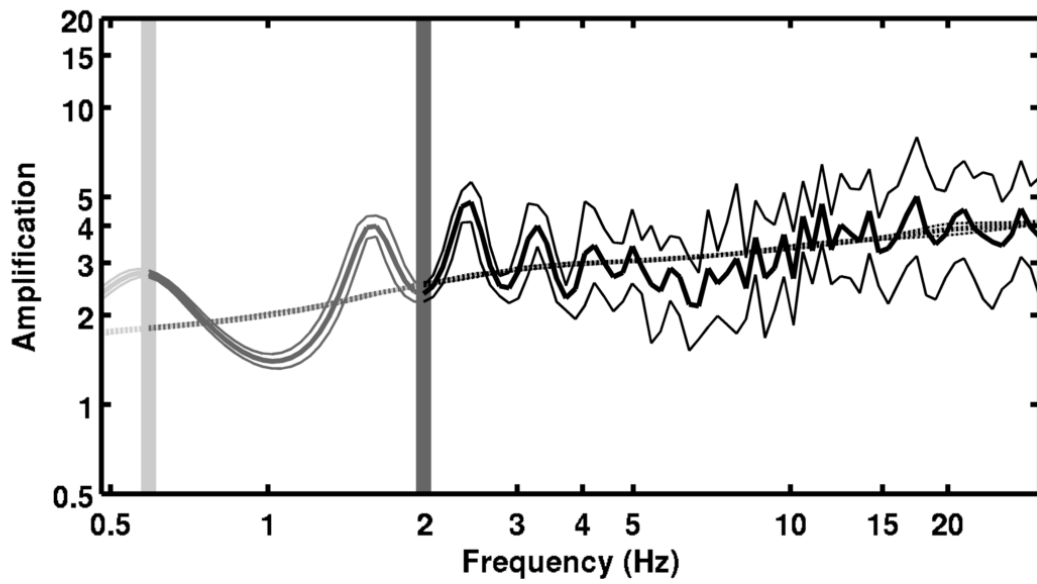


Figure 15: Theoretical SH transfer function (solid line) and quarter wavelength impedance contrast (dashed line) with their standard deviation. Significance of the greyshades is detailed in Fig. 14.

## 8 Conclusions

The array measurements presented in this study were successful in deriving a velocity model for the site of the SRHE station. Apart of the first few meters with low, unconstrained, velocities, we found a first layer of approximately 20 m with velocities of about 400 m/s corresponding to the alluvial terrace of the Wiese river. Below, the velocity in the molasse alsacienne is linearly increasing down to 100 m depth where it reaches 1000 m/s. The velocity is then not varying much down to the bedrock at about 500 m depth. The bedrock velocity is not constrained but assumed to be between 2000 and 2500 m/s. This interface with the Mesozoic rock is producing the fundamental peak in the ellipticity at 0.6 Hz.

$V_{s,30}$  is 373 m/s, which would corresponds to ground type B in the Eurocode 8, at the limit with type C [CEN, 2004]. The site would be classified in ground type E for the SIA261, although C would also be realistic [SIA, 2003]. The theoretical 1D SH transfer function and impedance contrast of the quarter-wavelength velocity computed from the inverted profiles show significant amplifications at clearly defined resonance frequencies. Recordings on the new station will allow to compare to these simple models.

## Acknowledgements

The authors thank Fr. Böhme who allowed the access to her park for the measurement.

## References

- Sylvette Bonnefoy-Claudet, Fabrice Cotton, and Pierre-Yves Bard. The nature of noise wavefield and its applications for site effects studies. *Earth-Science Reviews*, 79(3-4): 205–227, December 2006. ISSN 00128252. doi: 10.1016/j.earscirev.2006.07.004. URL <http://linkinghub.elsevier.com/retrieve/pii/S0012825206001012>.
- Jan Burjánek, Gabriela Gassner-Stamm, Valerio Poggi, Jeffrey R. Moore, and Donat Fäh. Ambient vibration analysis of an unstable mountain slope. *Geophysical Journal International*, 180(2):820–828, February 2010. ISSN 0956540X. doi: 10.1111/j.1365-246X.2009.04451.x. URL <http://gji.oxfordjournals.org/cgi/doi/10.1111/j.1365-246X.2009.04451.x><http://doi.wiley.com/10.1111/j.1365-246X.2009.04451.x>.
- J. Capon. High-Resolution Frequency-Wavenumber Spectrum Analysis. *Proceedings of the IEEE*, 57(8):1408–1418, 1969. ISSN 0018-9219. doi: 10.1109/PROC.1969.7278. URL <http://ieeexplore.ieee.org/lpdocs/epic03/wrapper.htm?arnumber=1449208>.
- CEN. *Eurocode 8: Design of structures for earthquake resistance - Part 1: General rules, seismic actions and rules for buildings*. European Committee for Standardization, en 1998-1: edition, 2004.
- Donat Fäh and Peter Huggenberger. INTERREG III Projekt: Erdbebenmikrozonierung am südlichen Oberrhein. Zusammenfassung. Technical report, Eidgenössische Technische Hochschule Zürich (ETHZ), 2006.
- Donat Fäh, Fortunat Kind, and Domenico Giardini. A theoretical investigation of average H / V ratios. *Geophysical Journal International*, 145:535–549, 2001.
- Donat Fäh, Gabriela Stamm, and Hans-Balder Havenith. Analysis of three-component ambient vibration array measurements. *Geophysical Journal International*, 172(1):199–213, January 2008. ISSN 0956540X. doi: 10.1111/j.1365-246X.2007.03625.x. URL <http://doi.wiley.com/10.1111/j.1365-246X.2007.03625.x><http://gji.oxfordjournals.org/cgi/doi/10.1111/j.1365-246X.2007.03625.x>.
- Donat Fäh, Marc Wathelet, Miriam Kristekova, Hans-Balder Havenith, Brigitte Endrun, Gabriela Stamm, Valerio Poggi, Jan Burjánek, and Cécile Cornou. Using Ellipticity Information for Site Characterisation. Technical report, NERIES JRA4 Task B2, 2009.
- Lukas Hauber. Ergebnisse der Geothermiebohrungen Riehen 1 und 2 sowie Reinach 1 im Südosten des Rheingrabens. *Geologisches Jahrbuch*, E 48:167–184, 1991.
- William B. Joyner, Richard E. Warrick, and Thomas E. Fumal. The effect of Quaternary alluvium on strong ground motion in the Coyote Lake, California, earthquake of 1979. *Bulletin of the Seismological Society of America*, 71(4):1333–1349, 1981.
- Katsuaki Konno and Tatsuo Ohmachi. Ground-Motion Characteristics Estimated from Spectral Ratio between Horizontal and Vertical Components of Microtremor. *Bulletin of the Seismological Society of America*, 88(1):228–241, 1998.

- Valerio Poggi and Donat Fäh. Estimating Rayleigh wave particle motion from three-component array analysis of ambient vibrations. *Geophysical Journal International*, 180(1):251–267, January 2010. ISSN 0956540X. doi: 10.1111/j.1365-246X.2009.04402.x. URL <http://doi.wiley.com/10.1111/j.1365-246X.2009.04402.x>.
- Valerio Poggi, Benjamin Edwards, and Donat Fäh. Characterizing the Vertical-to-Horizontal Ratio of Ground Motion at Soft-Sediment Sites. *Bulletin of the Seismological Society of America*, 102(6):2741–2756, December 2012a. ISSN 0037-1106. doi: 10.1785/0120120039. URL <http://www.bssaonline.org/cgi/doi/10.1785/0120120039>.
- Valerio Poggi, Donat Fäh, Jan Burjánek, and Domenico Giardini. The use of Rayleigh-wave ellipticity for site-specific hazard assessment and microzonation: application to the city of Lucerne, Switzerland. *Geophysical Journal International*, 188(3):1154–1172, March 2012b. ISSN 0956540X. doi: 10.1111/j.1365-246X.2011.05305.x. URL <http://doi.wiley.com/10.1111/j.1365-246X.2011.05305.x><http://gji.oxfordjournals.org/cgi/doi/10.1111/j.1365-246X.2011.05305.x>.
- J.M. Roesset. Fundamentals of soil amplification. In R. J. Hansen, editor, *Seismic Design for Nuclear Power Plants*, pages 183–244. M.I.T. Press, Cambridge, Mass., 1970. ISBN 978-0-262-08041-5. URL <http://mitpress.mit.edu/catalog/item/default.asp?tttype=2&tid=5998>.
- SIA. *SIA 261 Actions sur les structures porteuses*. Société suisse des ingénieurs et des architectes, Zürich, sia 261:20 edition, 2003.
- Marc Wathelet. An improved neighborhood algorithm: Parameter conditions and dynamic scaling. *Geophysical Research Letters*, 35(9):1–5, May 2008. ISSN 0094-8276. doi: 10.1029/2008GL033256. URL <http://www.agu.org/pubs/crossref/2008/2008GL033256.shtml>.